COLD-BASED GLACIATION ON MERCURY: ACCUMULATION AND FLOW OF ICE IN PERMANENTLY-SHADOWED CIRCUM-POLAR CRATER INTERIORS. J. L. Fastook[1] and J. W. Head[2], [1]University of Maine, Orono, ME, 04469, USA, fastook@maine.edu, [2]Brown University, Providence, RI, 02912, USA, James_Head@Brown.edu.

Introduction: Extensive radar **[*1*]** evidence exists for the presence of ice **[*2-9*]** in permanently shaded craters near the poles of Mercury **[*10,11*]**. Ice has been shown to be thermally stable under these conditions **[*12,13*]**, and a detailed energy-balance model **[*14*]** suggests an annual mean temperature near 110 K in permanent shade with surface temperatures close to 400 K in sunlit regions. Here we describe the dynamic properties of the proposed ice deposits to delineate the effects of ice deformation and the potential for flow that would modify these deposits in the time interval for which they are believed to have existed.

Modeling: We use a simple geometry, a function of crater diameter and latitude, that defines the shape of the crater walls and floor, as well as the permanently shaded volume that defines the ice surface. Depth of the crater is determined from the d/D ratio, 1:5 for craters less than 10 km in diameter and 1:25 for 100 km craters **[*14*]**. We define crater geometry with power-law fits **[*15*]**. An example based on Crater C, with a diameter of 50 km at a latitude of 87.5° is shown in Figure 1.

This configuration is passed to our ice dynamics model, a thermomechanical shallow-ice approximation model that has been used extensively both on Earth **[*16-18*]** and Mars **[*19-24*]**, here adapted for Mercury gravity.

An ablation rate of -1.0 m/yr is assumed in the sunlit areas, while minor accumulation (10^{-10} m/yr) is assumed for the ice surface **[*25*]**. With such a low accumulation rate the ice surface will basically "relax" into a configuration where the driving stress is minimized and any velocity is a result of internal deformation and not of mass-balance driven flux.

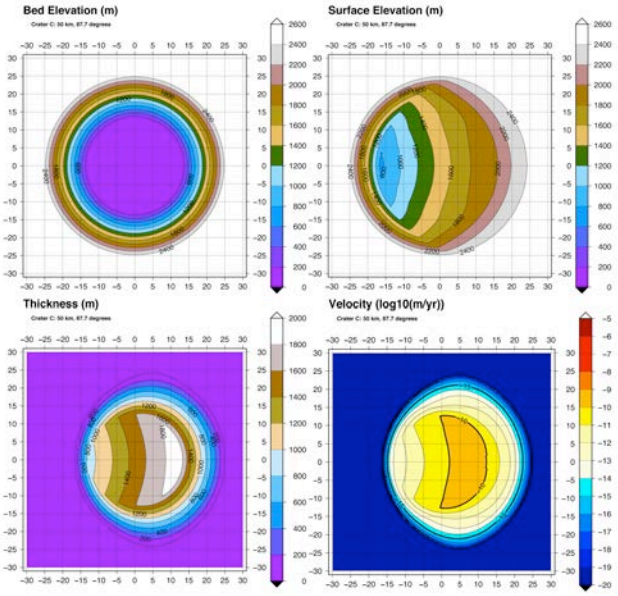

Figure 1: Geometry based on Talpe et al. (2012) and Crater C, with 50 km diameter at latitude 87.5°.

Thermodynamics: Boundary conditions for the thermodynamic component, used to calculate the ice hardness, include mean-annual surface temperature, taken to be 110 K, and basal heat flux. Because the ice is thin (basically the crater depth) and the slope is shallow (basically the sun angle), as well as the fact that the ice is cold, modeled velocities are very low, on the order of 10^{-10} m/yr for a uniform heat flux of 50 mW/m^2. Velocity, shown in Figure 1, is highest at the base of the crater wall where thickness is greatest. Long-term deformation with this velocity distribution would result in a thinning upstream toward the crater rim and a thickening downstream toward the crater center as the profile relaxes to a minimum driving stress configuration. However, with velocities this low little deformation would take place in the billion-year time span available.

Warmer ice is exponentially softer than colder ice **[*26-27*]**, and ice at depth is warmer than at the surface due to the insulating power of the ice. As such, the heat flux is a key parameter controlling ice deformation, and hence, ice velocity. Vasavada **[*14*]** uses an estimate for the heat flux of 20 mW/m^2 **[*28*]**. An estimate based on the height of a scarp and its implications for the depth of the brittle-ductile transition yields a surface heat flux that ranges from 30 to 60 mW/m^2 **[*29*]**.

Lateral Transport of Heat: An additional consideration is the lateral transport of heat from the warm sunlit surroundings of the cold shaded crater interior. A 2D solution of the steady-state heat flow equation **[*30*]** for a rectangular domain with a "cold spot" on the surface results in a depression of the isotherms below the cold spot. This depression and warping of the isotherms directs additional heat from the surroundings beneath the hot surface terrain into the center of the cooler region beneath the cold spot.

Temperature isotherms are bowed down beneath the cold spot, and since heat flows perpendicularly to the isotherms, heat is preferentially focused onto the base of the cold spot. The lateral flux is most intense beneath the edge of the crater, where the temperature discontinuity at the surface is largest. With a 10 km crater, the contributions from the edges overlap in the center, resulting in the largest flux at the center of the

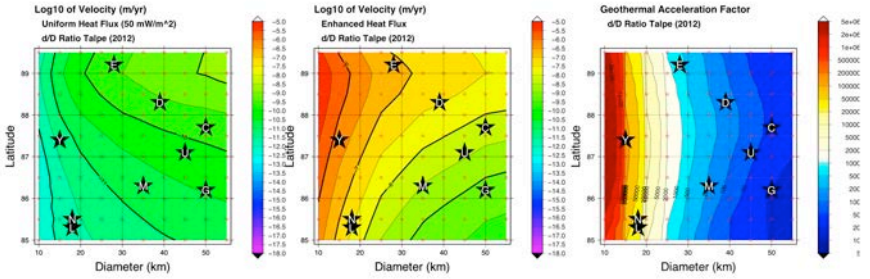

Figure 2: Base-10 log of velocity for the uniform flux case (left), the lateral heat transport case (center), and the ratios of these (right).

crater. Larger craters result in deeper penetration of the temperature anomaly, and hence steeper temperature gradients carrying more flux, but since the edges are farther apart, the synergistic contribution is less at the center and less lateral flux is delivered.

Results: To investigate the effect of the lateral heat flux, we run the ice sheet model for various crater sizes and latitudes (10 to 55 km in 5 km steps and 85 to 89.5^o in 0.5^o steps, a total of 100 model runs). Figure 2 shows the base-10 logarithm of the maximum velocity observed in each model run (a value of -10 corresponds to 10^{-10} m/yr) for the uniform flux case (left) as well as the non-uniform lateral heat transport case (center). Labelled stars indicates the position of craters with known deposits. Since depth depends on diameter, in the uniform flux case larger craters display faster velocities, primarily due to the thicker ice that can exist in the deeper craters. A secondary effect is the surface slope, which is steeper at lower latitudes. This effect is negated by the thinner ice available at the base of the crater walls with these steeper slopes, resulting in an optimal latitude at 89^o where the velocity is maximum for a given size crater. Lowest velocities are observed in the smallest craters at the lowest latitudes for the uniform heat flux case.

Given the significantly increased heat flux that can be delivered to the base of the crater by lateral transport, we re-apply the ice sheet model with these enhanced fluxes instead of the uniform 50 mW/m^2. With the same set of crater sizes and latitudes, but with the lateral heat transport, we obtain a very different looking pattern of velocities, (Figure 2 center). The much greater heat fluxes result in warmer ice, which being softer and easier to deform, yields higher velocities. The relative speedup due to this softer ice (Figure 2 right) is greatest for the smallest craters at the highest latitudes, reaching in some cases six orders of magnitude, attaining velocities of 10^{-5} m/yr. Even with large craters at low latitudes, where the warming is least, an order of magnitude speedup is observed. Large craters at high latitudes, where uniform-flux velocities are a maximum, experience a hundred-fold increase in velocity with the enhanced fluxes.

The highest velocities are observed in a 10 km crater at a latitude of 89^o, and Figure 3 shows the evolution of the ice surface in such a crater over a billion years. Thinning upstream and thickening downstream results in a flattening of the surface where the velocity is a maximum.

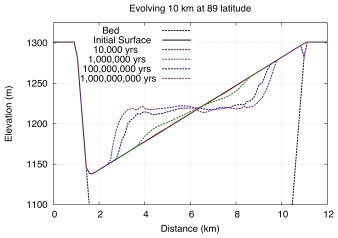

Figure 3: Evolution of a 10 km crater at 89^o, showing initial surface and deforming surface at 10^4, 10^6, 10^8, and 10^9 years.

Conclusions:

The thickest deposits with the greatest surface slope have the largest driving stresses as well as the warmest, softest ice at the bed, and hence the fastest velocities. However, accounting for the enhanced flux of heat from the surrounding hot sun-lit terrain is extremely important, offering orders of magnitude speedup over the uniform flux case, with the effect most pronounced for small craters where the greatest lateral heat flux is delivered to the centers of the craters. Even with the enhanced heat fluxes, the cold environment of the Mercury polar craters yields very small velocities and deformation is minimal on a time scale of millions of years. Even at it most rapid flow velocity, the ice surface would move only a kilometer in a hundred million years. These predictions can be used to compare to the observed deposit distributions and characteristics ***[10, 31-33]***.

References: ***1.*** Harmon J. (2007) *Space Sci. Rev.* 132, 307. ***2.*** Slade M et al. (1992) *Science*, 258, 635. ***3*** Harmon J and Slade M. (1992) *Science*, 258, 640. ***4.*** Butler B et al. (1995) *JGR*, 98, 15003. ***5*** Harmon J et al. (1994) *Nature*, 369, 213. ***6.*** Harmon J et al. (2011) *Icarus*, 211, 37. ***7.*** Lawrence D et al. (2013) *Science*, 339, 292. ***8.*** Neumann G et al. (2013) *Science*, 339, 296. ***9.*** Chabot N et al. (2014) *Geology*, 42, 1051. ***10.*** Chabot N et al. (2012) *GRL*, 39, L09204. ***11.*** Chabot N et al. (2013) *JGR (Planets)*, 118, 26. ***12.*** Paige D et al. (1992) *Science*, 258, 643. ***13.*** Paige D et al. (2013) *Science*, 339, 300. ***14.*** Vasavada A et al. (1999) *Icarus*, 141, 179. ***15.*** Talpe M et al. (2012) *JGR (Planets)*, 117, E00L13. ***16.*** Johnson J and Fastook J. (2002) *Quatern. Int.*, 95-96, 65. ***17.*** Kleman J et al. (2002) *Quatern. Int.*, 95-96, 87. ***18.*** Hooke R and Fastook J. (2007) *J. Glaciol.*, 53, 646. ***19.*** Fastook J et al. (2008) *Icarus*, 198, 305. ***20.*** Fastook J et al. (2011) *Icarus*, 216, 23. ***21.*** Fastook J et al. (2012) *Icarus*, 219, 25. ***22.*** Fastook J et al. (2013) *Icarus*, 228, 54. ***23.*** Fastook J and Head J. (2014) *Planet. Space Sci.*, 91, 60. ***24.*** Fastook J and Head J. (2015) *Planet. Space Sci.*, 106, 82. ***25.*** Moses J et al. (1999) *Icarus*, 137, 197. ***26.*** Glen J. In Tison L, ed., (1958) *Physics of the Movement of Ice*, 47, 171. ***27.*** Paterson W and Budd W. (1982) *Cold Reg. Sci. and Technol.*, 6, 175. ***28.*** Schubert G et al. In Vilas F et al, eds., (1988) *Mercury*, 429. ***29.*** Nimmo F and Watters T. (2004) *GRL*, 31, L02701. ***30.*** Becker E et al. (1981) *Finite Elements, An Introduction*. Prentice-Hall. ***31.*** Deutsch A et al. (2016) *LPS47*. ***32.*** Deutsch A et al. (2016) *Icarus*, submitted. ***33***. Chabot N et al. (2016) LPS47.